FULL PAPER

Efficiency Enhancement of Organic Light-Emitting Diodes Incorporating a Highly Oriented Thermally Activated Delayed Fluorescence Emitter

*Christian Mayr, Sae Youn Lee, Tobias D. Schmidt, Takuma Yasuda, Chihaya Adachi, and Wolfgang Brütting**

An organic light-emitting diode (OLED) with the blue emitter CC2TA showing thermally activated delayed fluorescence (TADF) is presented exhibiting an external quantum efficiency (η_{EQE}) of 11% ± 1%, which clearly exceeds the classical limit for fluorescent OLEDs. The analysis of the emission layer by angular dependent photoluminescence (PL) measurements shows a very high degree of 92% horizontally oriented transition dipole moments. Excited states lifetime measurements of the prompt fluorescent component under PL excitation yield a radiative quantum efficiency of 55% of the emitting species. Thus, the radiative exciton fraction has to be significantly higher than 25% due to TADF. Performing a simulation based efficiency analysis for the OLED under investigation allows for a quantification of individual contributions to the efficiency increase originating from horizontal emitter orientation and TADF. Remarkably, the strong horizontal emitter orientation leads to a light-outcoupling efficiency of more than 30%.

1. Introduction

Organic light-emitting diodes (OLEDs) have been investigated for almost three decades[1] and significant progress in this field has been made so far. Recent years have seen first applications in general lighting, but especially for flat-panel displays with their brilliant colors, high viewing angles, and the possibility to fabricate them on flexible substrates, the use of OLEDs offers many advantages.

An important value characterizing the efficiency of OLEDs is the external quantum efficiency:[2]

$$\eta_{EQE} = \gamma \eta_r q_{eff} \eta_{out} = \eta_{int} \eta_{out} \quad (1)$$

In this equation γ represents the charge carrier balance, η_r is the fraction of excitons that is allowed to decay radiatively by spin statistics, and q_{eff} is the effective radiative quantum efficiency specifying the fraction of spin allowed excited states that actually decay by emitting a photon. q_{eff} is derived from the intrinsic radiative quantum efficiency q by a modification induced by the OLED cavity due to the Purcell effect.[3–6] The last factor η_{out}, finally, is the light-outcoupling efficiency, which is used to extract the internal quantum efficiency η_{int}.

For fluorescent molecules, the radiative exciton fraction η_r is typically assumed to be 0.25.[7,8] By the introduction of phosphorescent emitters, this value could be increased to 1.[9–11] However, due to the need for rare metals like iridium or platinum, which facilitate efficient spin-orbit coupling, an increase of fabrication costs for the OLED device is very likely.[12–14] For a long time the outcoupling efficiency has been believed to be around 0.2.[15] Thus, the classical limit of η_{EQE} of OLEDs using fluorescent and phosphorescent emitters is 5% and 20%, respectively. Recently, promising concepts enabling an enhancement of device efficiency beyond these limits have been introduced: the conversion of non-radiative triplets to radiative singlets as well as horizontal emitter orientation.

The former is especially observed for emitters exhibiting triplet-triplet-annihilation (TTA)[16,17] and thermally activated delayed fluorescence (TADF). Recently, TADF emitters have drawn a lot of attention to themselves and many new molecules with this behaviour have been synthesized.[18–22] By molecular design, it is possible to spatially separate the highest occupied molecular orbital (HOMO) and lowest unoccupied molecular orbital (LUMO), causing a decrease of the energy gap ΔE_{ST} between the lowest excited singlet (S_1) and triplet (T_1) state. This enables the efficient conversion of triplet to singlet excitons by reverse intersystem crossing (RISC), which is a temperature activated mechanism. Because the emission originates from the S_1 state, this mechanism is sometimes termed singlet harvesting.[20] It is thus possible to enhance the fluorescence efficiency of OLEDs by an increase of the radiative exciton fraction. Therewith, OLEDs with η_{EQE} values far beyond the classical limit and comparable to devices using phosphorescent emitters have been reported.[22]

Another concept for the improvement of device efficiency is the use of oriented molecules. The aforementioned number of

C. Mayr, Dr. T. D. Schmidt, Prof. W. Brütting
Institute of Physics, University of Augsburg
86135, Augsburg, Germany
E-mail: Wolfgang.Bruetting@physik.uni-augsburg.de
S. Y. Lee, Prof. T. Yasuda, Prof. C. Adachi
Center for Organic Photonics and
Electronics Research (OPERA)
Kyushu University
744 Motooka, Nishi, Fukuoka 819–0395, Japan

DOI: 10.1002/adfm.201400495

0.2 outcoupling efficiency is typically achieved if isotropically oriented emitters are employed in thickness optimized devices. Horizontally oriented emitters, however, show a significantly increased outcoupling efficiency due to a reduced coupling to surface plasmons at the organic/cathode interface.[3,23–25] Theoretically, it is possible to increase η_{EQE} up to 46% for perfectly horizontally oriented emitters without the use of external outcoupling structures.[26] Practically, 30.2% have been reached with the partially horizontally oriented green emitter $Ir(ppy)_2(acac)$, which is the highest number ever achieved for a single emission layer OLED up to date.[26] However, phosphorescent emitters for the deep blue spectral region show low stability with short lifetimes during electrical operation in devices. Thus, fluorescent emitters are commonly employed in so-called hybrid white OLEDs to cover the blue wavelength region.

In this study, we show that both concepts to improve device efficiency can be combined in the sky-blue emitting TADF molecule 2,4-bis{3-(9 *H*-carbazol-9-yl)-9 *H*-carbazol-9-yl}-6-phenyl-1,3,5-triazine (**CC2TA**) doped into the host bis[2-(diphenylphosphino)phenyl]ether oxide (DPEPO). In order to perform an efficiency analysis of OLEDs, the precise knowledge of the radiative quantum efficiency and outcoupling efficiency is mandatory. We measure the molecular orientation of the transition dipole moments of the emitter species doped in the host DPEPO and determine its prompt fluorescent lifetime on a series of samples with varying distance between the emission layer and a highly reflective mirror layer in order to extract the radiative quantum efficiency. A simulation based efficiency analysis of OLEDs incorporating the TADF emitter allows for a precise determination of the radiative exciton fraction and to figure out the contributions to the enhanced efficiency originating from TADF and horizontal emitter orientation.

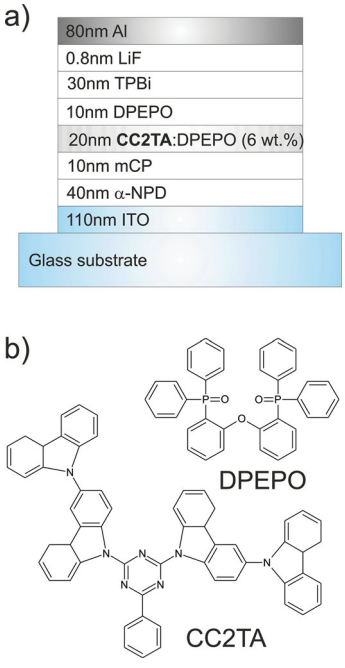

Figure 1. a) Stack layout of the device under investigation and b) molecular structures of the used materials in the emitting layer: **CC2TA** acts as a TADF emitter and DPEPO as a host.

2. Results and Discussion

The OLED investigated in this study incorporates the emitter **CC2TA**, which has a small singlet-triplet energy gap of $\Delta E_{ST} = 0.06$ eV only, facilitating efficient RISC from T_1 to S_1 and showing delayed fluorescence.[27] The OLED has the following stack layout as depicted in **Figure 1**: glass/110 nm indium tin-oxide (ITO)/40 nm 4,4′-bis [*N*-(1-naphthyl)-*N*-phenyl]biphenyldiamine (α-NPD)/10 nm 1,3-bis(N-carbazolyl) benzene (mCP)/20 nm (DPEPO) doped with **CC2TA** at 6 wt%/10 nm DPEPO/30 nm 1,3,5-tris(N-phenylbenzimidazol-2-yl)benzene (TPBi)/0.8 nm LiF/80 nm Al.

The OLED exhibits a sky-blue emission with a peak emission wavelength of 490 nm at a current density of 1 mA cm^{-2}. A maximum η_{EQE} of 11% ± 1% is reached at a current density of 0.01 mA cm^{-2} (see **Figure 2**), which by far exceeds the classical limit for fluorescent OLEDs. In the following, the emission layer of the OLED will be analyzed in terms of molecular orientation and radiative quantum efficiency in order to quantify the contributions to the enhanced efficiency of the device.

2.1. Determination of the Transition Dipole Moment Orientation

The determination of the orientation of the optical transition dipole moments of the emitter **CC2TA** doped into the host DPEPO was performed by analyzing the angular dependent photoluminescence (PL) spectrum (see **Figure 3**a).[28] The sample consisted of a 15 nm thick film of DPEPO doped with **CC2TA** (6 wt%) on a glass substrate that was attached to a fused silica prism on a rotation stage and excited by a laser with a wavelength of 375 nm. The PL intensity was detected as a function of the angle to the surface normal and the wavelength between 400 nm and 650 nm. In this measurement, only the p-polarized emission yields information about the orientation. It contains contributions of both the horizontal p_x and the vertical p_z transition dipole moments (with respect to the coordinate system shown in the inset of **Figure 4**). The s-polarized emission, however, originates only from the horizontal p_y transition dipole moments, and thus, does not contain information about the relation between horizontal and vertical orientation. The degree of emitter orientation can be characterized by the anisotropy factor Θ which is defined as the fraction of the vertically oriented to the total amount of transition dipole moments:[29]

$$\Theta = \frac{[p_z]}{[p_x]+[p_y]+[p_z]} \quad (2)$$

By using optical simulations, the angular dependent emission spectra can be calculated. The simulation is based on a dipole ensemble embedded in a multilayer stack and uses a transfer-matrix formalism calculating the Fresnel reflection and transmission coefficients at each interface.[30,31] In Figure 3b,c the simulated angular dependent p-polarized emission for a completely isotropic ($\Theta = 1/3$) and completely horizontal ($\Theta = 0$) orientation of the transition dipole moments is shown, respectively. The emission at angles higher than 41° corresponds to substrate modes, which are outcoupled by the prism, and differences of molecular orientation are clearly visible in that angular

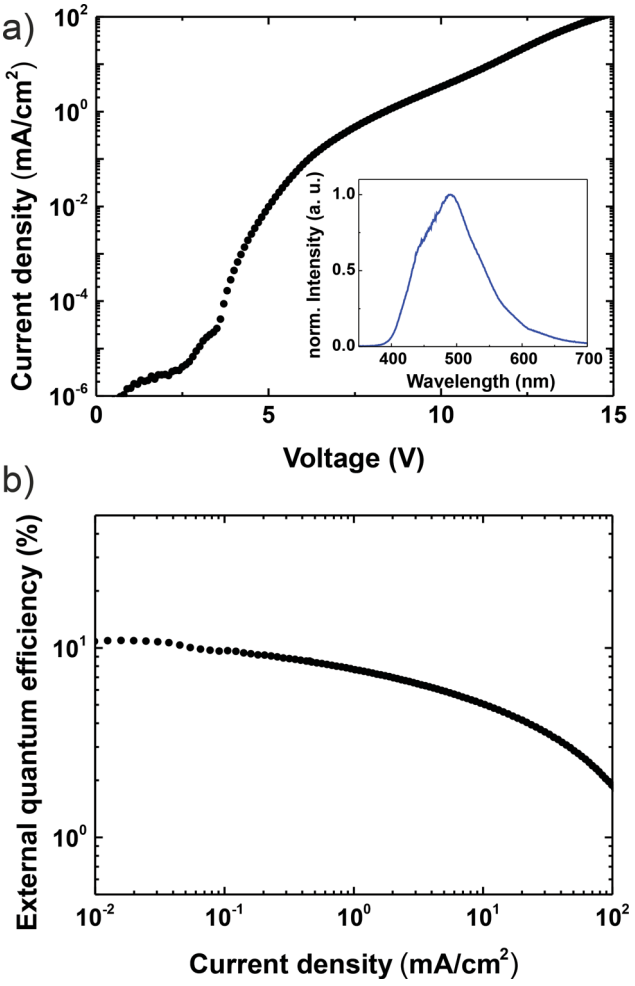

Figure 2. a) Current density-voltage characteristics (inset: electroluminescence spectrum at a current density of 1 mA cm^{-2}) and b) external quantum efficiency η_{EQE} for the OLED stack shown in Figure 1a.[27]

region for both cases. It is obvious that the isotropic emitter orientation is not consistent with the measurement. For a better comparability of simulation and measurement, the cross-sections at the peak-wavelength of 470 nm are shown in Figure 4.

The best fit yields an anisotropy factor $\Theta = 0.18 / 2.18 = 0.08$ (i.e., $[p_z] = 0.18$, $[p_x] = [p_y] = 1$ in Equation (2)), corresponding to only 8% vertically and thus 92% horizontally oriented transition dipole moments. In **Figure 5** the ground-state optimized molecular structure of **CC2TA** is shown. Even though the carbazole units are slightly twisted at the position of the nitrogen atoms (especially the outermost carbazole units), the molecule extends mainly in the *x*-*y*-plane (with respect to the coordinate system defined in Figure 5) resulting in a predominantly planar structure. In order to correlate the orientation of the transition dipole moments with the molecular frame, a time dependent (TD) density functional theory (DFT)-calculation has been performed on GAUSSIAN 03[32] by using the B3LYP functional with the 6–31G(d,p) basis set. The calculation yields two almost equivalent transition dipole moments both directed between the bicarbazole and triazine unit on which the HOMO and LUMO are distributed, respectively.[25] Thus, light-emission originates from electron transfer from the triazine unit to one of the two bicarbazole units with almost equivalent probability. Since the two directions of the transition dipole moments define a plane, which is almost coincident with the *x*-*y*-plane, we ascribe the high degree of horizontal orientation to the mainly planar structure of the molecule. Horizontal orientation of a planar molecule is energetically favoured due to a higher intermolecular interaction between guest and host molecules during film growth. In this case the guest follows the same trend as neat films, where for linear or planar-shaped molecules a general tendency to adopt horizontal orientation has been observed.[33–36]

The DFT calculation also predicts a singlet-triplet gap of $\Delta E_{ST} = 0.06$ eV[27] which is in very good agreement with the experimental result of $\Delta E_{ST} = 0.05$ eV (see Supporting Information, Part S1).

2.2. Determination of the Intrinsic Radiative Quantum Efficiency

For the determination of the radiative quantum efficiency q in Equation (1), typically the PL quantum efficiency Φ_{PL} of thick organic films on a fused silica substrate or dissolved in solvents is measured in an integrating sphere.[37] However, if oriented emitter molecules are involved, the amount of light

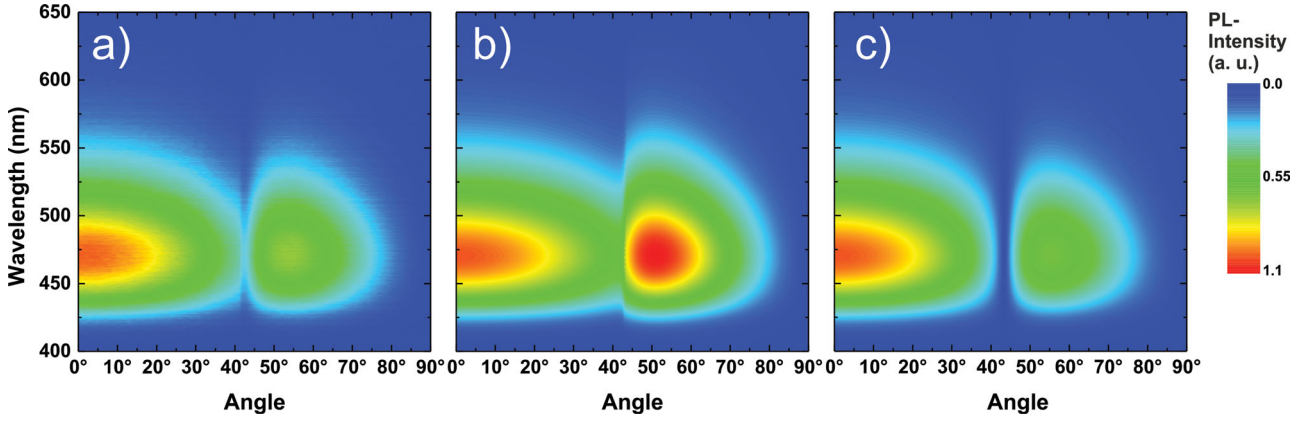

Figure 3. P-polarized angular dependent emission spectra of a film of 15 nm DPEPO doped with **CC2TA** (6 wt%) on a glass substrate. a) Experimental data together with b) simulated data for a perfectly isotropic orientation of the transition dipole moments (Θ = 1/3), c) simulated data for a perfectly horizontal (Θ = 0) orientation of the transition dipole moments. The emission intensity has been normalized at an emission angle of 0°.

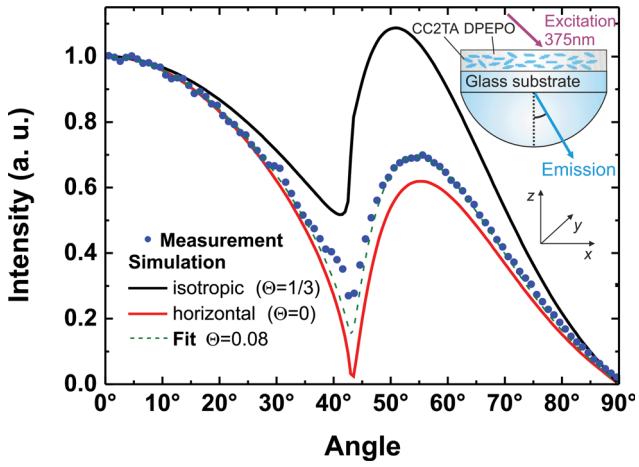

Figure 4. Cross-section of the angular dependent p-polarized PL emission spectra shown in Figure 3 at a wavelength of 470 nm. (The polarization of light is given with respect to an observer in the *x*-*z*-plane.) The black and the red curve represent the simulation for perfectly isotropic (Θ = 1/3) and horizontal (Θ = 1/3) orientation of the transition dipole moments, respectively. The measured data have been fitted (green dashed line) to an orientation of Θ = 0.08, corresponding to 92% horizontally oriented transition dipole moments in the film.

that is radiated from the film is larger than in the isotropic case (see Supporting Information, Part S2). Thus, disregarding the orientation of the emitter in the film will lead in general to erroneous results for the quantum efficiency as well as for an OLED efficiency analysis.

An alternative approach to determine the radiative quantum efficiency of an emitter that does not rely on the measurement of absolute intensities in an integrating sphere, is to analyze the excited states lifetimes of the emitter in an optical microcavity, e.g., an OLED with an electron transport layer (ETL) of varying thickness.[29–31,38]

Here, we present a method that uses an even more simplified stack layout. The intrinsic radiative quantum efficiency q of an emitter in the absence of an optical cavity is defined as

$$q = \frac{\Gamma_r}{\Gamma_r + \Gamma_{nr}}, \tag{3}$$

where Γ_r and Γ_{nr} are the radiative and non-radiative decay rates of the emitting molecule, respectively. Taking a cavity (e.g., due to metal electrodes or other interfaces) into account, the radiative rate Γ_r (and consequently the radiative quantum efficiency) is modified by the Purcell effect according to $\Gamma_r^* = F\Gamma_r$, with F being the Purcell factor.[3–6] This change of the radiative rate leads to an effective radiative quantum efficiency q_{eff} in the cavity environment. The Purcell factor F depends on the refractive indices and thicknesses of the layer stack as well as the emission spectrum of the material. Additionally, the Purcell factor is also affected by the orientation of the transition dipole moment of the emitting molecules and can be calculated by the weighted sum of the Purcell factors corresponding to the three orthogonal orientations (*x*,*y*, and *z*).[29] Accordingly, the lifetimes of the excited states are $\tau_0 = (\Gamma_r + \Gamma_{nr})^{-1} \equiv \Gamma_0^{-1}$ in the absence of a cavity and $\tau = (F\Gamma_r + \Gamma_{nr})^{-1} \equiv \Gamma^{-1}$ with cavity. Thus the relative change of excited states lifetimes can be expressed as

$$\frac{\tau}{\tau_0} = \frac{\Gamma_0}{\Gamma} = \frac{1}{Fq + (1-q)}. \tag{4}$$

This expression can be used to determine the (intrinsic) radiative quantum efficiency q of an emitter on a series of samples, where the microcavity environment, i.e., the Purcell factor, and therefore the lifetime of the emitter is systematically varied. The following stack layout has been used: glass/20 nm **CC2TA**:DPEPO (6 wt%)/x nm 1,4-bis(triphenylsilyl)benzene (UGH-2)/100 nm Ag. By using this stack layout, the radiative

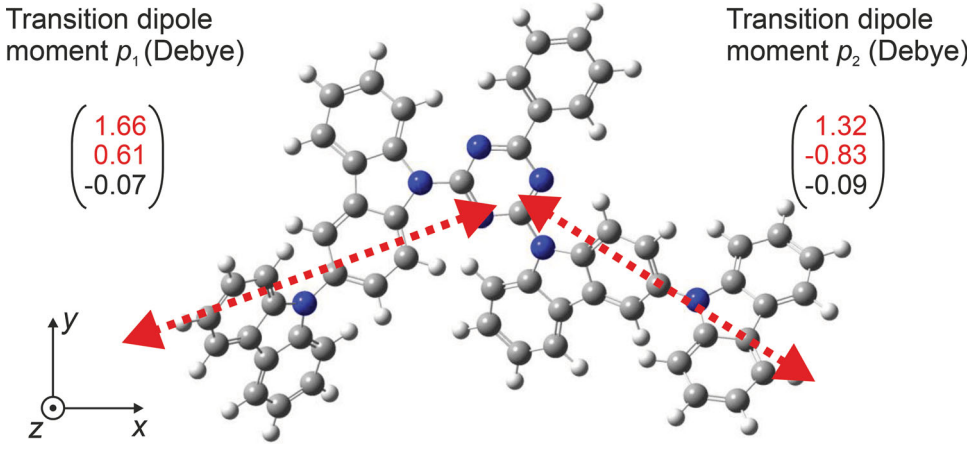

Figure 5. Optimized molecular structure of **CC2TA** and transition dipole moments calculated by TD-DFT B3LYP/6–31+G(d,p) for the lowest transition from the ground (S_0) to the excited state (S_1) originating from two possible transitions with almost equivalent transition probabilities (oscillator strength $f = 0.0348$ for p_1 and $f = 0.0268$ for p_2). The molecule extends mainly in the *x*-*y*-plane (extension in the *x*-direction: 2.19 nm, *y*-direction: 1.42 nm, and *z*-direction: 0.73 nm), thus having a predominantly planar structure. The plane defined by the two transition dipole moments almost coincides with the *x*-*y*-plane.

rate of the fluorescent decay of the emitter is modified by a variation of its distance to the reflecting Ag mirror. Thereby, UGH-2 with varying layer thickness acts as an inert optical spacer between the emitting molecules and the reflective Ag mirror.[39]

The samples have been excited by a pulsed nitrogen laser with a wavelength of 337 nm under a nitrogen atmosphere and the decay of the prompt fluorescence has been detected by a streak camera system. Please note that the prompt fluorescent decay on a nanosecond time scale is not affected by TADF processes because these involve time scales of microseconds. In that sense, intersystem crossing from the excited singlet to the triplet state will also be treated as a non-radiative process.

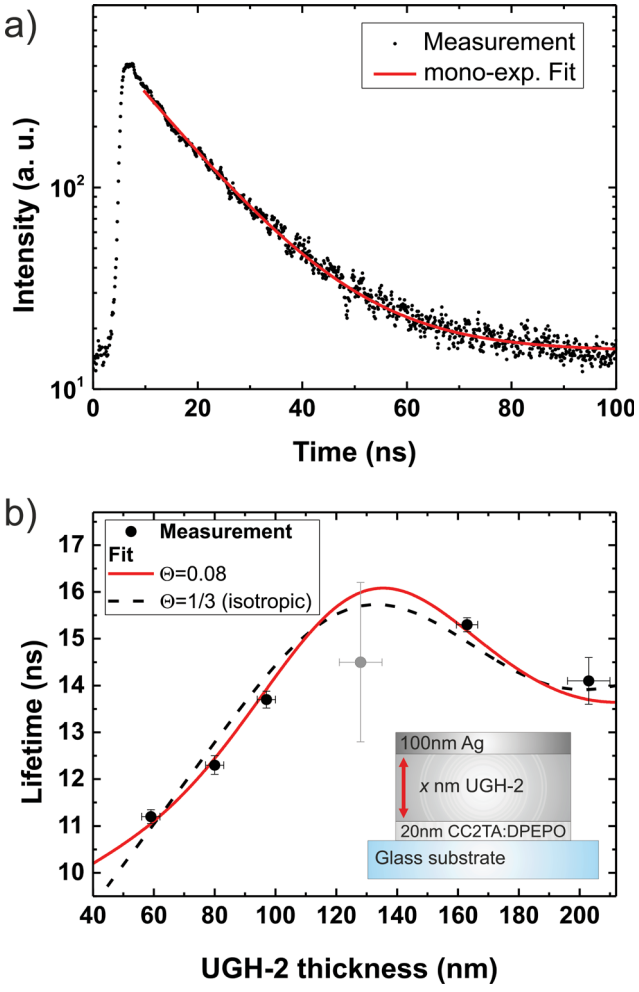

Figure 6. Determination of the intrinsic radiative quantum efficiency q of **CC2TA** by analyzing the excited states lifetimes of the prompt fluorescence of a series of samples with a varying distance between the emitting layer and the reflective Ag mirror upon PL excitation. The samples have the following stack layout: glass/20 nm **CC2TA**:DPEPO (6 wt%)/x nm UGH-2/100 nm Ag. a) Exemplary prompt fluorescent decay of a sample with 97 nm UGH-2. The monoexponential fit (red curve) yields a lifetime $\tau = (13.7 \pm 0.1)$ ns. b) Lifetime data for samples with varying UGH-2 thickness and fits according to Equation (4) to the measurements, assuming mainly horizontal ($\Theta = 0.08$, red curve) and completely isotropic ($\Theta = 1/3$, dashed black line) emitter orientation. The fit for mainly horizontal orientation yields $q = 0.55 \pm 0.04$ and an intrinsic excited states lifetime of $\tau_0 = (14.2 \pm 0.1)$ ns. Note that another data point at a UGH-2 thickness of 129 nm (grey data point) was disregarded in the lifetime analysis because of an ambiguous lifetime fit owing to strongly depressed emission at the cavity minimum for horizontal emitters.

In **Figure 6**a, an exemplary fluorescent decay of the prompt component is shown together with a mono-exponential fit. Figure 6b summarizes the lifetime data for the different samples with a varying spacer thickness. The data have been fitted with Equation (4) using Purcell factors that have been calculated according to optical simulations, taking into account the measured anisotropic ($\Theta = 0.08$) emitter orientation as well as a hypothetical isotropic emitter orientation ($\Theta = 1/3$) for comparison. Especially for small spacer thicknesses, where the orientation of the emitter strongly influences the coupling to surface plasmons, the obtained fit for the mainly horizontal orientation of the emitter shows a much better agreement with the measured lifetime data. A similar trend has been observed in the literature.[29] With the intrinsic radiative quantum efficiency q and lifetime τ_0 as free parameters, the best fit has been achieved for $q = 0.55 \pm 0.04$ and $\tau_0 = (14.2 \pm 0.1)$ ns. The presented method offers a straight-forward way of determining the intrinsic radiative quantum efficiency q. The q value, which is extracted from time-resolved PL measurements, is in good agreement with the PL quantum efficiency $\Phi_{PL} = 0.62$ measured in an integrating sphere (ref. [27], if the predominantly horizontal emitter orientation is taken into account (see Supporting Information, Part S2).

2.3. OLED Efficiency Analysis

In order to quantify the contributions to the enhanced efficiency of the investigated OLED, a precise knowledge of all factors determining η_{EQE} is necessary. By assuming a charge carrier balance close to the upper limit ($\gamma \leq 1$), Equation (1) can be rewritten as

$$\eta_r \geq \frac{\eta_{int}}{q_{eff}} = \frac{\eta_{EQE}}{q_{eff}\eta_{out}} \quad (5)$$

giving an expression for the radiative exciton fraction. As discussed above, η_{EQE} and the radiative quantum efficiency q_{eff} are accessible by measurement, but the outcoupling efficiency η_{out}, which especially depends on the molecular orientation of the emitting molecules, must be obtained by numerical simulation. In previous work η_{out} has been assumed to be around 0.2 for OLEDs incorporating TADF emitters.[19,27] However, if horizontally oriented emitters are present in a device, this value can reach over 0.3.[3,23–26] Thus, according to Equation (5), disregarding emitter orientation can lead to an overestimation of both η_{int} and η_r by a factor of around 1.5 or even more.

Coming back to the OLEDs under investigation here (Figure 1), we can now use the knowledge of the orientation of the emitting molecule **CC2TA** and the radiative quantum efficiency q to perform a comprehensive efficiency analysis.

Optical simulations yield the fraction of power for the emission to air, where the refractive indices and thicknesses of the multilayer structure of the OLED, the emission spectrum, and the emitter orientation were taken into account. The

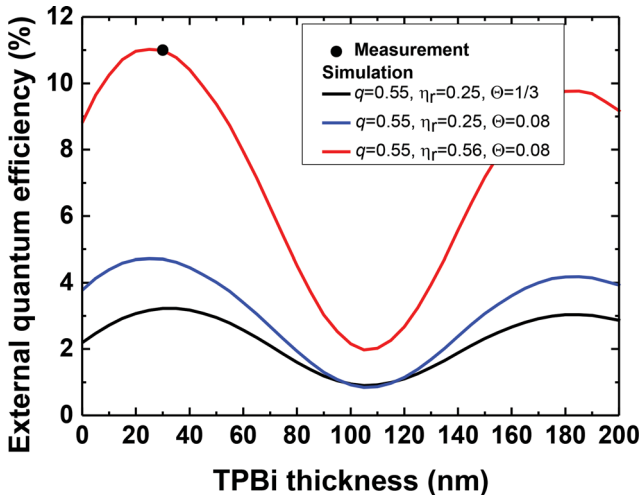

Figure 7. Calculated external quantum efficiency η_{EQE} for the OLED stack shown in Figure 1 with varying TPBi thickness. Assuming a perfect charge balance factor ($\gamma = 1$), isotropic emitter orientation ($\Theta = 1/3$) and disregarding TADF ($\eta_r = 0.25$), a maximum η_{EQE} of only 3.4% can be anticipated (black curve). However, the measured efficiency of the OLED clearly exceeds the classical limit for fluorescent OLEDs. The predominantly horizontal emitter orientation ($\Theta = 0.08$, blue curve) enhances the light-outcoupling efficiency and accounts for an efficiency increase by a factor of 1.46. Additionally, due to TADF, the radiative exciton fraction η_r is determined to be at least 0.56 (red curve), boosting η_{int} by another factor of 2.24.

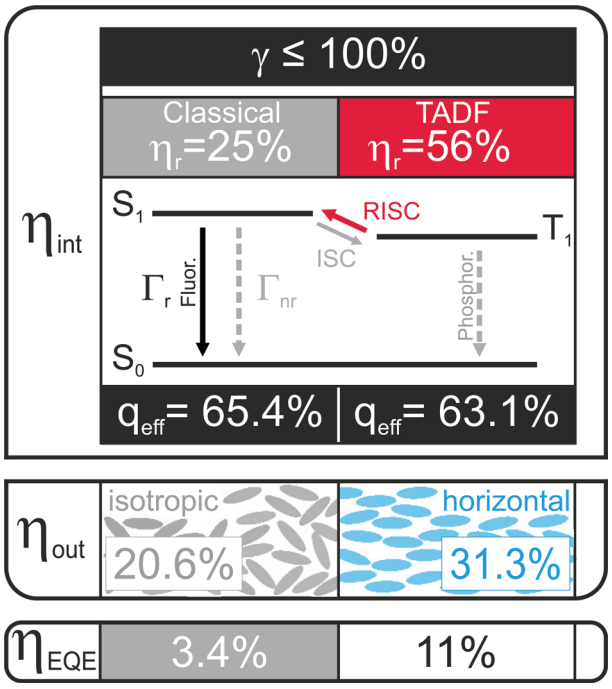

Figure 8. Individual contributions to the efficiency for the investigated OLED: The left column gives the numbers for an isotropic singlet emitter, while the numbers to the right are valid for an oriented TADF emitter enabling external quantum efficiency beyond the classical limit. TADF enhances the radiative exciton fraction η_r due to up-conversion of triplet excitons to the singlet state, which in turn boosts the internal quantum efficiency η_{int}. Additionally, the horizontal orientation of the transition dipole moments in the emission layer increases the outcoupling efficiency η_{out}. In both scenarios, the same radiative quantum efficiency of the emitter ($q = 0.55$) was assumed, however, owing to an orientation dependent Purcell factor, slightly different q_{eff} -values have to be taken in the calculation of η_{EQE} .

emission zone has been assumed to be located at the mCP/DPEPO interface. In **Figure 7** the calculated η_{EQE} for a varying ETL thickness is shown for different contributions of its constituting factors according to Equation (1). The thickness of the ETL strongly influences the efficiency due to changing interference conditions and the microcavity environment. As can be seen, the stack layout of the investigated OLED with a TPBi thickness of 30 nm is well-optimized for maximum light outcoupling. For an intrinsic radiative quantum efficiency of $q = 0.55$, isotropic emitter orientation and disregarding TADF ($\eta_r = 0.25$), a maximum η_{EQE} of only 3.4% can be expected at the given ETL thickness. However, the high experimental value of $\eta_{EQE} = 11\%$ clearly exceeds the calculated one. In order to explain this discrepancy, the individual contributions to η_{EQE} have to be figured out. As discussed in section 2.1, the orientation of the transition dipole moments is not isotropic but mainly horizontal with respect to the substrate. If this is taken into account, optical simulations yield an outcoupling efficiency of $\eta_{out} = 0.313$ (instead of $\eta_{out} = 0.206$ for the isotropic case, due to a higher coupling to surface plasmons) and lead to η_{EQE} of 4.9%. Furthermore, the radiative rate is enhanced in the microvacity environment of the OLED, resulting in an effective radiative quantum efficiency $q_{eff} = 0.631$ ($q_{eff} = 0.654$ for the isotropic case), according to an orientation dependent Purcell effect.[29] Thus, both effects together lead to an efficiency boost by a factor of 1.46. However, horizontal orientation of the emitter alone cannot explain the high value of the measured η_{EQE}. To explain the experimental result, the radiative exciton fraction η_r must be higher than 0.25. Taking the measured η_{EQE} together with η_{out} and q_{eff} as determined above, the lower limit can be calculated as $\eta_r \geq 0.56$, according to Equation (5). Hence, the internal quantum efficiency η_{int} for this OLED is 35.1% and is significantly lower than by assuming an isotropic emitter orientation, which yields $\eta_{int} = 53{,}2\%$ (or 56% according to ref. [27]). Consequently, the impact of TADF is overestimated by not taking horizontal emitter orientation into account. A summary of the individual contributions to the electroluminescent process can be seen in **Figure 8**. The high η_{EQE} can be attributed to two reasons: First, the contribution of TADF of **CC2TA** emitter molecules up-converts triplet excitons to the singlet state, boosting the internal quantum efficiency η_{int} by a factor of 2.24. Second, the horizontal orientation of the transition dipole moments enhances η_{EQE} by a factor of 1.46 due to an increased light outcoupling. Thus, instead of 3.4% efficiency for an isotropic singlet emitter, the TADF OLED with horizontal emitter orientation reaches η_{EQE} of 11%. Unlike, e.g., iridium-complexes with an octahedral molecular structure, TADF emitters are preferential candidates for strong non-isotropic orientation of the transition dipole moments, because they have a much higher degree of freedom in terms of molecular design. Even though **CC2TA** already experiences almost the maximum efficiency enhancement due to horizontal orientation, the efficiency of OLEDs incorporating

TADF emitters can be further increased by the synthesis of new molecules with even smaller ΔE_{ST} (increasing RISC and thus η_r) and a high value of q. Thus, we believe that by using TADF emitters with a high radiative quantum efficiency, high RISC rate, and strong horizontal orientation with respect to the substrate, the efficiency and lifetime of blue OLEDs can be tremendously enhanced and the search for stable blue phosphorescent emitters might become redundant.

3. Conclusions

An OLED incorporating the sky-blue emitting TADF molecule **CC2TA** doped into a DPEPO matrix as the emitting layer exhibited a high η_{EQE} of 11% ± 1%, exceeding the classical limit for fluorescent emitters. The analysis of the emitter orientation of **CC2TA** showed that 92% of its transition dipole moments were horizontally oriented with respect to the substrate, which can be ascribed to the mainly planar molecular structure. The (intrinsic) radiative quantum efficiency of the prompt fluorescence has been determined as $q = 0.55 \pm 0.04$. By analyzing the efficiency of the OLED by optical simulations, a radiative exciton fraction $\eta_r \geq 0.56$ and an outcoupling efficiency of $\eta_{out} = 0.313$ have been identified. The efficiency enhancement by TADF and horizontal emitter orientation can be precisely quantified: For the investigated OLED, TADF accounts for an increase of the internal quantum efficiency η_{int} by a factor of 2.24 and the horizontal molecular orientation for another factor of 1.46 in terms of extracting the light to the outside world. This finding highlights the possibility of combining two very promising concepts for efficiency improvement, enabling the fabrication of OLEDs far exceeding the classical limit for fluorescent devices. Due to the lack of stable phosphorescent blue emitters, oriented TADF emitters can play a key role in the development of high efficiency white OLEDs in the future.

4. Experimental Section

Sample Fabrication: All substrates were degreased with distilled water, a neutral detergent, acetone, and isopropyl alcohol and cleaned in a UV-ozone chamber (NLUV253, Nippon Laser and Electrics Lab.) before they were loaded into an evaporation system. The organic layers were thermally evaporated on the substrates under a vacuum with a pressure of $<3 \times 10^{-4}$ Pa with an evaporation rate of <0.3 nm s^{-1}. For OLED devices, a glass substrate precoated with a 110-nm-thick ITO layer with a sheet resistance of < 20 Ω/□ was used. An aluminum (Al) layer as the cathode was deposited through a 1 mm-diameter opening in a shadow mask. Samples for the orientation measurement and for time-resolved lifetime measurements have been encapsulated with a glass slide using epoxy glue in a nitrogen atmosphere to prevent degradation upon laser excitation.

Materials: The molecule **CC2TA** has been synthesized according to ref. [27]. α-NPD, mCP, DPEPO, TPBi, LiF, Al, and UGH-2 have been purchased from commercial suppliers.

Sample Characterization: To determine the molecular orientation in doped films, angular-dependent PL measurements have been performed.[26] The sample consisted of a glass substrate with 15 nm DPEPO doped with 6 wt% **CC2TA**. The sample was attached to a fused silica half cylinder prism by index matching liquid and the emission angle was changed by the use of a rotation stage. The spectra were measured using a fibre optical spectrometer (SMS-500, Sphere Optics) and a polarizing filter to distinguish between p- and s-polarized light. The excitation of the samples was performed with a 375 nm cw laser diode with a fixed excitation angle of 45°. Time resolved PL measurements have been performed with a streak camera system (C5680, Hamamatsu) and spectrograph (Acton SpectraPro 2300i, Princeton Instruments). The excitation signal was synchronized with the streak camera system by a multichannel delay generator (Stanford Research Systems DG535). The excitation has been performed with a nitrogen laser (MNL 200, Laser Technik Berlin) with a wavelength of 337 nm and a pulse length of 700 ps. Film thicknesses of the UGH-2 spacer have been determined by both variable angle spectroscopic ellipsometry (VASE) (SE850, Sentech Instruments) and profilometry (DEKTAK 8, Veeco Instruments) on silicon substrates coated in the same evaporation process as the samples for time-resolved measurements. For the determination of the optical constants of the organic films, a spectroscopic ellipsometer (M-2000U, J. A. Woollam Co., Inc.) was used and the ellipsometric parameters Ψ and Δ were analyzed by "WVASE32" software (J. A. Wollam Co., Inc.).

The current-density and voltage (J-V) characteristics of OLEDs were measured using a semiconductor parameter analyser (E52373A, Agilent Technologies Inc.). The EL spectra were recorded by a multi-channel analyser (SD2000, Ocean Optics) at a current density of 1 mA cm^{-2}. The luminance of the OLEDs was measured using an optical powermeter (1930C, Newport Co.). The η_{EQE} was calculated from the current-density, luminance, and EL spectrum assuming a Lambertian emission profile.

Supporting Information

Supporting Information is available from the Wiley Online Library or from the author.

Acknowledgements

The authors acknowledge financial support from the Bayerische Forschungsstiftung, the Japanese Society for the Promotion of Science (JSPS), and from the Deutsche Forschungsgemeinschaft (DFG) under contract no. BR 1728/13–1. S.Y. L. acknowledges financial support by the Funding Program for World-Leading Innovative R & D on Science and Technology (FIRST). Futhermore, the authors want to thank Dr. Q. Zhang for helpful discussions and Dr. T. Komino for support with ellipsometric measurements.

Received: February 12, 2014
Revised: April 15, 2014
Published online: June 11, 2014

[1] C. W. Tang, S. A. VanSlyke, *Appl. Phys. Lett.* **1987**, *51*, 913.
[2] T. Tsutsui, E. Aminaka, C. P. Lin, D.-U. Kim, *Phil. Trans. R. Soc. London A* **1997**, *355*, 801.
[3] S. Nowy, B. C. Krummacher, J. Frischeisen, N. A. Reinke, W. Brütting, *J. Appl. Phys.* **2008**, *104*, 123109.
[4] H. Becker, S. E. Burns, R. H. Friend, *Phys. Rev. B* **1997**, *56*, 1893.
[5] B. C. Krummacher, S. Nowy, J. Frischeisen, M. Klein, W. Brütting, *Org. Electron.* **2009**, *10*, 478.
[6] X.-W. Chen, W. C. H. Choy, C. J. Liang, P. K. A. Wai, S. He, *Appl. Phys. Lett.* **2007**, *91*, 221112.
[7] M. A. Baldo, D. F. O'Brien, M. E. Thompson, S. R. Forrest, *Phys. Rev. B* **1999**, *60*, 14422.
[8] M. Segal, M. A. Baldo, R. J. Holmes, S. R. Forrest, Z. G. Soos, *Phys. Rev. B* **2003**, *68*, 075211.

[9] M. A. Baldo, D. F. O'Brien, Y. You, A. Shoustikov, S. Sibley, M. E. Thompson, S. R. Forrest, *Nature* **1998**, *395*, 151.
[10] J. S. Wilson, A. S. Dhoot, A. J. A. B. Seeley, M. S. Khan, A. Köhler, R. H. Friend, *Nature* **2001**, *413*, 828.
[11] Y. Sun, N. C. Giebink, H. Kanno, B. Ma, M. E. Thompson, S. R. Forrest, *Phys. Rev. B* **1999**, *60*, 14422.
[12] C. Adachi, M. A. Baldo, M. E. Thompson, S. R. Forrest, *J. Appl. Phys.* **2001**, *90*, 5048.
[13] D. F. O'Brien, M. A. Baldo, M. E. Thompson, S. R. Forrest, *Appl. Phys. Lett.* **1999**, *74*, 442.
[14] M. A. Baldo, S. Lamansky, P. E. Burrows, M. E. Thompson, S. R. Forrest, *Appl. Phys. Lett.* **1999**, *75*, 4.
[15] K. Meerholz, D. C. Müller, *Adv. Funct. Mater.* **2001**, *11*, 251.
[16] C. Ganzorig, M. Fujihira, *Appl. Phys. Lett.* **2002**, *81*, 3137.
[17] D. Kondakov, *J. Appl. Phys.* **2007**, *102*, 114504.
[18] A. Endo, M. Ogasawara, A. Takahashi, D. Yokoyama, Y. Kato, C. Adachi, *Adv. Mater.* **2009**, *21*, 4802.
[19] A. Endo, K. Sato, K. Yoshimura, T. Kai, A. Kawada, H. Miyazaki, C. Adachi, *Appl. Phys. Lett.* **2011**, *98*, 083302.
[20] R. Czerwieniec, J. Yu, H. Yersin, *Inorg. Chem.* **2011**, *50*, 8293.
[21] M. J. Leitl, F.-R. Küchle, H. A. Mayer, L. Wesemann, H. Yersin, *J. Phys. Chem. A* **2013**, *117*, 11823.
[22] H. Uoyama, K. Goushi, K. Shizu, H. Nomura, C. Adachi, *Nature* **2012**, *492*, 234.
[23] W. H. Weber, C. F. Eagen, *Opt. Lett.* **1979**, *4*, 236.
[24] J. Frischeisen, D. Yokoyama, A. Endo, C. Adachi, W. Brütting, *Org. Electron.* **2011**, *12*, 809.
[25] M. Flämmich, J. Frischeisen, D. S. Setz, D. Michaelis, B. C. Krummacher, T. D. Schmidt, W. Brütting, N. Danz, *Org. Electron.* **2011**, *12*, 1663.
[26] S.-Y. Kim, W.-I. Jeong, C. Mayr, Y.-S. Park, K.-H. Kim, J.-H. Lee, C.-K. Moon, W. Brütting, J.-J. Kim, *Adv. Funct. Mater.* **2013**, *23*, 3896.
[27] S. Y. Lee, T. Yasuda, H. Nomura, C. Adachi, *Appl. Phys. Lett.* **2012**, *101*, 093306.
[28] J. Frischeisen, D. Yokoyama, C. Adachi, W. Brütting, *Appl. Phys. Lett.* **2010**, *96*, 073302.
[29] T. D. Schmidt, D. S. Setz, M. Flämmich, J. Frischeisen, D. Michaelis, B. C. Krummacher, N. Danz, W. Brütting, *Appl. Phys. Lett.* **2011**, *99*, 163302.
[30] W. Brütting, J. Frischeisen, T. D. Schmidt, B. J. Scholz, C. Mayr, *Phys. Status Solidi A* **2012**, *210*, 44.
[31] T. D. Schmidt, B. J. Scholz, C. Mayr, W. Brütting, *IEEE J. Sel. Top. Quantum Electron.* **2013**, *19*, 7800412.
[32] M. J. Frisch, G. W. Trucks, H. B. Schlegel, G. E. Scuseria, M. A. Robb, J. R. Cheeseman, J. A. Montgomery, Jr., T. Vreven, K. N. Kudin, J. C. Burant, J. M. Millam, S. S. Iyengar, J. Tomasi, V. Barone, B. Mennucci, M. Cossi, G. Scalmani, N. Rega, G. A. Petersson, H. Nakatsuji, M. Hada, M. Ehara, K. Toyota, R. Fukuda, J. Hasegawa, M. Ishida, T. Nakajima, Y. Honda, O. Kitao, H. Nakai, M. Klene, X. Li, J. E. Knox, H. P. Hratchian, J. B. Cross, V. Bakken, C. Adamo, J. Jaramillo, R. Gomperts, R. E. Stratmann, O. Yazyev, A. J. Austin, R. Cammi, C. Pomelli, J. W. Ochterski, P. Y. Ayala, K. Morokuma, G. A. Voth, P. Salvador, J. J. Dannenberg, V. G. Zakrzewski, S. Dapprich, A. D. Daniels, M. C. Strain, O. Farkas, D. K. Malick, A. D. Rabuck, K. Raghavachari, J. B. Foresman, J. V. Ortiz, Q. Cui, A. G. Baboul, S. Clifford, J. Cioslowski, B. B. Stefanov, G. Liu, A. Liashenko, P. Piskorz, I. Komaromi, R. L. Martin, D. J. Fox, T. Keith, M. A. Al-Laham, C. Y. Peng, A. Nanayakkara, M. Challacombe, P. M. W. Gill, B. Johnson, W. Chen, M. W. Wong, C. Gonzalez, J. A. Pople, Gaussian 03, Revision D.01, Gaussian, Inc., Wallingford, CT **2004**.
[33] D. Yokoyama, A. Sakaguchi, M. Suzuki, C. Adachi, *Appl. Phys. Lett.* **2008**, *93*, 173302.
[34] D. Yokoyama, A. Sakaguchi, M. Suzuki, C. Adachi, *Appl. Phys. Lett.* **2009**, *95*, 243303.
[35] D. Yokoyama, A. Sakaguchi, M. Suzuki, C. Adachi, *Org. Electron.* **2009**, *10*, 127.
[36] J. Y. Kim, D. Yokoyama, C. Adachi, *J. Phys. Chem. C* **2012**, *116*, 8699.
[37] J. C. de Mello, H. F. Wittmann, R. H. Friend, *Adv. Mater.* **1997**, *9*, 230.
[38] T. D. Schmidt, D. S. Setz, M. Flämmich, J. Frischeisen, D. Michaelis, C. Mayr, A. F. Rausch, T. Wehlus, B. J. Scholz, T. C. G. Reusch, N. Danz, W. Brütting, *Appl. Phys. Lett.* **2013**, *103*, 093303.
[39] K. H. Drexhage, *J. Lumin.* **1970**, *1–2*, 693.